AGU PUBLICATIONS

Geophysical Research Letters

RESEARCH LETTER
10.1002/2016GL068710

Key Points:
- The Mississippi River is an important N_2O source throughout the ice-free period
- The N_2O:NO_3^- mass ratio is nonlinear, implying an upper bound on N_2O concentrations
- A doubling of riverine NO_3^- would increase N_2O emissions by about 40%

Correspondence to:
P. A. Turner,
turne289@umn.edu

Citation:
Turner, P. A., T. J. Griffis, J. M. Baker, X. Lee, J. T. Crawford, L. C. Loken, and R. T. Venterea (2016), Regional-scale controls on dissolved nitrous oxide in the Upper Mississippi River, *Geophys. Res. Lett.*, *43*, 4400–4407, doi:10.1002/2016GL068710.

Received 10 DEC 2015
Accepted 20 APR 2016
Accepted article online 22 APR 2016
Published online 6 MAY 2016

Regional-scale controls on dissolved nitrous oxide in the Upper Mississippi River

P. A. Turner[1], T. J. Griffis[1], J. M. Baker[1,2], X. Lee[3,4], J. T. Crawford[5], L. C. Loken[6,7], and R. T. Venterea[1,2]

[1]Department of Soil, Water, and Climate, University of Minnesota, Twin Cities, St. Paul, Minnesota, USA, [2]Agricultural Research Service, United States Department of Agriculture, St. Paul, Minnesota, USA, [3]School of Forestry and Environmental Studies, Yale University, New Haven, Connecticut, USA, [4]Yale-Nanjing University of Information, Science and Technology Center on Atmospheric Environment, Nanjing University of Information and Technology, Nanjing, China, [5]National Research Program, United States Geological Survey, Boulder, Colorado, USA, [6]Wisconsin Water Science Center, United States Geological Survey, Middleton, Wisconsin, USA, [7]Center for Limnology, University of Wisconsin-Madison, Madison, Wisconsin, USA

Abstract The U.S. Corn Belt is one of the most intensive agricultural regions of the world and is drained by the Upper Mississippi River (UMR), which forms one of the largest drainage basins in the U.S. While the effects of agricultural nitrate (NO_3^-) on water quality in the UMR have been well documented, its impact on the production of nitrous oxide (N_2O) has not been reported. Using a novel equilibration technique, we present the largest data set of freshwater dissolved N_2O concentrations (0.7 to 6 times saturation) and examine the controls on its variability over a 350 km reach of the UMR. Driven by a supersaturated water column, the UMR was an important atmospheric N_2O source (+68 mg N_2O N m^{-2} yr^{-1}) that varies nonlinearly with the NO_3^- concentration. Our analyses indicated that a projected doubling of the NO_3^- concentration by 2050 would cause dissolved N_2O concentrations and emissions to increase by about 40%.

1. Introduction

The Upper Mississippi River (UMR) drains nearly 492,000 km^2 of the U.S. Corn Belt [*Natural Resources Conservation Service*, 2012], one of the most intensively cultivated regions on the planet. Within the UMR basin, more than half of the U.S. share of nitrogen (N) fertilizers are applied [*Griffis et al.,* 2013; *Food and Agriculture Organization*, 2015] to produce 40% of the nation's corn [*NRCS*, 2012]. These activities have amplified river N loading, mainly as nitrate (NO_3^-) [*Turner and Rabalais*, 1991; *Panno et al.,* 2006]. Much effort has focused on the effects of excessive N on water quality [*Rabalais*, 2002] and the ability of the UMR to reduce downstream transport [*Richardson et al.,* 2004; *Strauss et al.,* 2004, 2011] to estuary systems. However, measurements of nitrous oxide (N_2O), the dominant stratospheric ozone-depleting substance [*Ravishankara et al.,* 2009] and an important greenhouse gas [*Hartmann et al.,* 2013], in the UMR are conspicuously absent in the literature, representing a significant knowledge gap in our understanding of the regional controls on dissolved N_2O concentrations and emissions in heavily modified agricultural rivers.

Rivers are globally significant sources of N_2O to the atmosphere [*Beaulieu et al.,* 2011; *Turner et al.,* 2015], responsible for 10%–17% of the anthropogenic budget [*Beaulieu et al.,* 2011; *Syakila and Kroeze*, 2011]. Yet rivers remain one of the most uncertain N_2O sources [*Nevison*, 2000], largely due to low spatiotemporal sampling resolution that is unable to resolve the high variability of surface water N_2O concentrations caused by dynamic production and consumption processes. Nitrous oxide production via denitrification and nitrification in the water column [*Beaulieu et al.,* 2010] and sediments [*Boyer et al.,* 2006; *Marzadri et al.,* 2014] causes rivers to become saturated with N_2O that is emitted to the atmosphere. Generally, the degree of N_2O saturation increases with the concentration of NO_3^- and ammonium (NH_4^+), indicating that emissions from large rivers are derived from in situ N_2O production [*Beaulieu et al.,* 2010] rather than terrestrial delivery. Global model simulations suggest a doubling of N loading in rivers by the year 2050 [*Seitzinger et al.,* 2002], implying that N_2O emissions from rivers, including the UMR, will likely increase. However, the relationship between dissolved N_2O concentrations in rivers and N loading is poorly constrained because obtaining these types of data is logistically challenging and, consequently, observations are very limited.

Recent studies indicate that surface water N_2O concentrations behave nonlinearly, plateauing in response to a number of environmental drivers, including dissolved oxygen concentration [*Rosamond et al.,* 2012] and

water temperature [*Venkiteswaran et al.,* 2014]. Observations that N_2O concentrations increase at a decreasing rate are likely caused by the inverse relation between N loading and removal efficiency [*Mulholland et al.,* 2008]. This nonlinearity implies that N_2O emissions will not increase proportionally with N loading projections, especially as a river becomes N saturated. Characterizing the N_2O:NO_3^- mass ratio should provide an upper constraint on N_2O concentrations in N-rich systems and provide insights regarding how these rivers may respond under business-as-usual N scenarios.

Here we present the largest freshwater dissolved N_2O concentration data set to date and the first N_2O surface water concentration measurements from the UMR to (1) explore the biochemical factors that control the degree of riverine N_2O saturation, (2) identify N_2O hot spots, and (3) predict how N_2O concentrations will respond to future N loading.

2. Materials and Methods

2.1. Site Description

For this study, we considered a portion of the UMR that extends from Minneapolis, MN, through Pool 8 (near La Crosse, WI). Along this stretch, eight lock and dam combinations have been installed to facilitate navigation. The river is organized into pools to describe river sections between two neighboring dams. In addition to the main channel, a pool includes impounded waters, side channels, and backwaters [*Strauss et al.,* 2011]. The temporal (10 April, 16 June, 4 August, and 13 October) and spatial dynamics of N_2O concentration were observed in Pool 8, a 104 km^2 section of the UMR upstream of Lock and Dam 8. From 1 to 3 August 2015, a 350 km reach from Minneapolis, Minnesota, to Pool 8 provided a regional-scale assessment of N_2O concentration patterns in the UMR.

2.2. Water Sampling

We used a boat-mounted flow-through sampling system [*Crawford et al.,* 2015] to continually measure surface water N_2O and other limnological parameters. In brief, we pumped surface water (0.3 m) to a series of sensors and stripped the dissolved gases using a sprayer-type equilibration device [*Crawford et al.,* 2015]. This type of equilibrator has a fast response time [*Santos et al.,* 2012; *Yoon et al.,* 2016] and has been used in oceanic N_2O campaigns [*Bange et al.,* 1996; *Arévalo-Martínez et al.,* 2013, 2015; *O'Reilly et al.,* 2015] but has never been used to measure N_2O in freshwater systems. Equilibrator headspace air was drawn through a desiccant tube before entering a Teledyne gas filter correlation N_2O analyzer (Model M320EU2; Teledyne Instruments, City of Industry, CA, USA) [*Fassbinder et al.,* 2013; *Turner et al.,* 2015]. A circular loop was created by returning sample air back to the equilibrator device. A data logger (Model 23X; Campbell Scientific, Logan, UT, USA) recorded the N_2O analyzer output at 1 Hz for postprocessing.

This system, the Fast Limnology Automated Measurement (FLAMe) platform, has been used extensively to monitor dissolved CO_2 and CH_4 on the Mississippi River [*Crawford et al.,* 2016]. The FLAMe instrument panel consisted of a YSI sonde (Model EXO2; Yellow Springs, OH, USA), an optical NO_3^- sensor (Model SUNA V2, Satlantic, Halifax, NS, Canada), and a GPS device. The FLAMe platform measured water temperature (*T*), dissolved oxygen (DO), pH, turbidity, specific conductivity, Chl *a*, and fluorescent dissolved organic matter (fDOM). Higher fDOM values are related to terrestrially derived organic matter [*Spencer et al.,* 2013] and are a proxy for dissolved organic carbon [*Crawford et al.,* 2015]. Spatial coordinates were recorded semicontinuously at 1 Hz, while measurements of NO_3^- were recorded at 0.1 Hz.

2.3. Data Processing

The raw N_2O concentration data ($n = 101{,}862$) were processed using MATLAB (R2013b; Mathworks, Natick, MA, USA) software. To georeference the FLAMe and N_2O data, we determined the hydraulic and sensor response time lags using a series of step change experiments [*Crawford et al.,* 2015]. The hydraulic and sensor lag describes the time required for the instrument to detect a step change (42.3 s) caused by tube length, instrument responsivity, and equilibrator lag. The sensor responsivity of the N_2O analyzer was estimated using an equilibrator time constant τ (61.6 s) that describes the time required for a 63% step change to occur. A wavelet denoising technique was applied to the N_2O concentration data to improve the signal-to-noise ratio of the signal [*Fassbinder et al.,* 2013]. For convenience of data processing and statistical analyses, all of the data streams were subjected to 30 s block averaging resulting in a data series of $n = 3667$.

The surface water N_2O concentration ($[N_2O]$; mol N_2O L^{-1}) was calculated from

$$[N_2O] = [N_2O_*] \times F(T, p) \quad (1)$$

where $[N_2O_*]$ is the equilibrator concentration and $F(T, p)$ is the solubility function at the given surface water temperature (T) and pressure (p) [*Weiss and Price*, 1980; *Grefe and Kaiser*, 2014]. The theoretical equilibrium N_2O concentration ($[N_2O_{amb}]$, mol N_2O L^{-1}) assuming water-atmosphere equilibrium was calculated similarly

$$[N_2O_{amb}] = [N_2O_{amb}*] \times F(T, p) \quad (2)$$

where $[N_2O_{amb}*]$ is the ambient atmospheric concentration reading by the N_2O analyzer and $F(T, p)$ is the solubility function. The ambient concentration was measured every 2 h. The analyzer was zeroed and spanned using analytical grade standards (Specialty Gases of America, Toledo, OH, USA) before each measurement campaign. The concentration precision after wavelet denoising is 1.5 nmol mol^{-1} [*Fassbinder et al.,* 2013]. These two metrics, $[N_2O]$ and $[N_2O_{amb}]$, are water temperature dependent. Therefore, we use their ratio to standardize the measurements with respect to the in situ water temperature as N_2O saturation (N_2O_{sat})

$$N_2O_{sat} = \frac{[N_2O]}{[N_2O_{amb}]} \quad (3)$$

A novel aspect of the FLAMe platform is its capacity to incorporate spatial coordinates to identify spatial patterns driving N_2O_{sat} across large spatial distances. A Getis-Ord G* analysis of each data set identified clustering of statistically significant high and low N_2O_{sat} and NO_3^- values relative to neighboring points [*Ord and Getis*, 2010]. A 99% significance threshold was used to determine N_2O_{sat} and NO_3^- hot spots and cold spots (Arcmap v.10.3; ESRI, Redlands, CA, USA).

Using CO_2 piston velocity (k) measurements from the UMR [*Crawford et al.,* 2016], we estimated the mean ($n = 22$) k using the temperature-adjusted N_2O Schmidt number [*Wanninkhof*, 1992]. Nitrous oxide fluxes (nmol $N_2O - N$ m^{-2} s^{-1}) from the UMR were calculated as

$$Flux_{N2O} = k \times ([N_2O - N_2O_{amb}]) \quad (4)$$

We assumed that variations in the evasion coefficient would be negligible within the UMR because of minimal channel geometry change [*Wallin et al.,* 2011], and consequently, N_2O_{sat} and $Flux_{N2O}$ would be most sensitive to in situ production and consumption mechanisms [*Beaulieu et al.,* 2015]. We estimated that N_2O_{sat} ratios greater than 1.2 and less than 0.8 were indicative of active production and consumption zones, respectively, while N_2O_{sat} values within this window were classified as zones of negligible production and consumption [*Beaulieu et al.,* 2015].

2.4. Ensemble Regression Trees

The controls on riverine N_2O_{sat} were identified independently for each river section using ensemble ($n = 500$) binary bagged regression trees with the MATLAB *fitensemble* function (v.2015.b, Mathworks, Natick, MA, USA). This supervised learning method does not require an assumption of normality, and the bootstrap aggregation technique reduces prediction variance [*De'ath and Fabricius*, 2000; *Sutton*, 2005] making it a powerful tool for better understanding the controls on N_2O saturation [*Baulch et al.,* 2011; *Venkiteswaran et al.,* 2014; *Lundy et al.,* 2015]. The relative predictor importance (RPI) of each explanatory variable on the corresponding N_2O_{sat} response was computed by summing the change in mean square error from splitting each predictor and dividing by the number of nodes. The importance was normalized with respect to the largest value [*Lundy et al.,* 2015]; a response of 1 recognizes the independent variable with the greatest impact on the N_2O_{sat}, and a value of 0 indicates no influence. The variance of the ensemble regression model was determined by calculating the pseudo R^2 value of model predicted and observed N_2O_{sat} ratios.

3. Results and Discussion

The UMR was supersaturated with N_2O throughout the ice-free measurement period, indicating it was an important atmospheric source (Figures 1 and 2a). Across all sampling locations and dates, the mean (standard deviation) N_2O_{sat} was 2 (0.9) times the atmospheric saturation (Table 1). The mean (standard deviation) fluxes at the regional scale (August) and throughout the ice-free period (April–October) were 0.5 (0.2) and

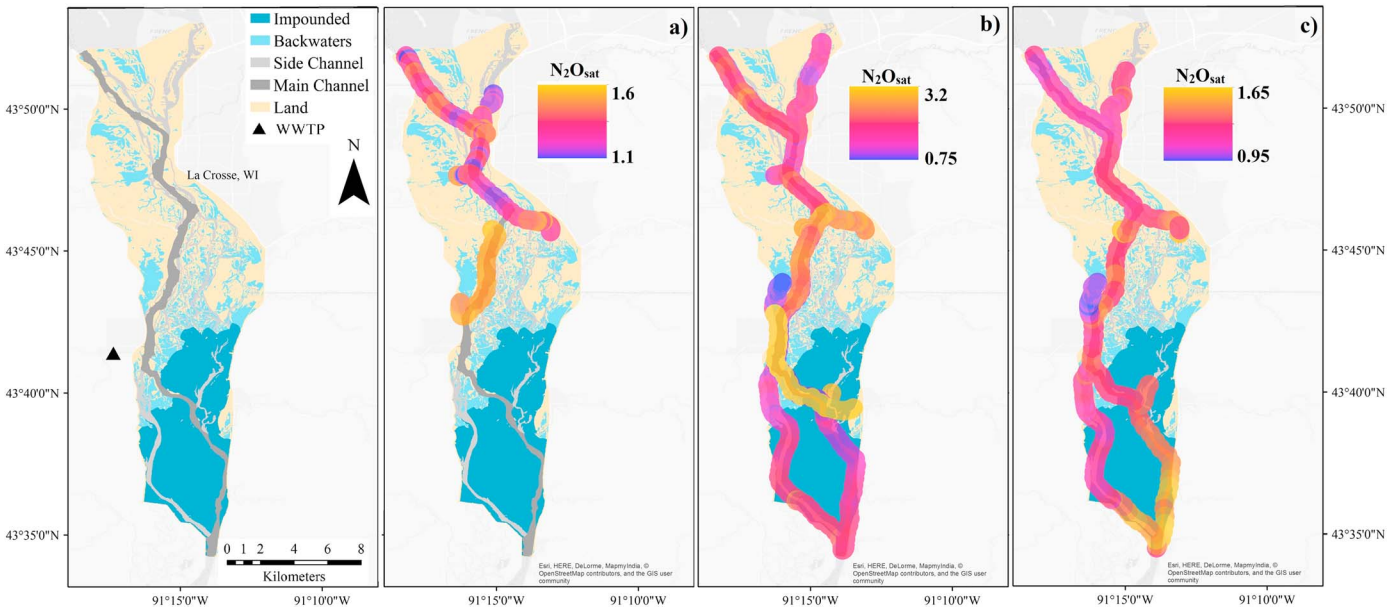

Figure 1. The temporal and spatial dynamics of N_2O_{sat} in Pool 8 of the UMR in (a) April ($n = 298$), (b) August ($n = 828$), and (c) October ($n = 514$).

0.2 (0.1) nmol N_2O N m^{-2} s^{-1}, respectively, which are comparable to observations from nearby corn fields [*Griffis et al.*, 2013] and within the range observed in other large rivers [*McMahon and Dennehy*, 1999; *Cole and Caraco*, 2001; *Hinshaw and Dahlgren*, 2013]. Integrated over the measurement period (186 days), the UMR emitted 68 (20–115) mg N_2O −N m^{-2}. Because groundwater and most tributary flows are negligible in a river of this size, and because of the short residence time of upstream dissolved gases, our data indicate that the UMR actively produces N_2O throughout the year. Although, at certain times and places, external N_2O inputs could be significant, for instance, high discharge from the N-rich Minnesota River could affect N_2O_{sat}, but these sources are poorly constrained.

During the June Pool 8 campaign, an instrument issue prevented N_2O_{sat} measurements greater than 4.8. Because we can only state that N_2O_{sat} was equal to or above 4.8, they were not included in the following analyses. However, the high N_2O_{sat} in Pool 8 in June is consistent with recent top-down measurements and modeling that found total emissions (direct + indirect) [*Miller et al.*, 2012; *Griffis et al.*, 2013] and indirect emissions from leaching and runoff [Chen et al., under review] to be the highest during this period, likely because of the recent application of N fertilizers.

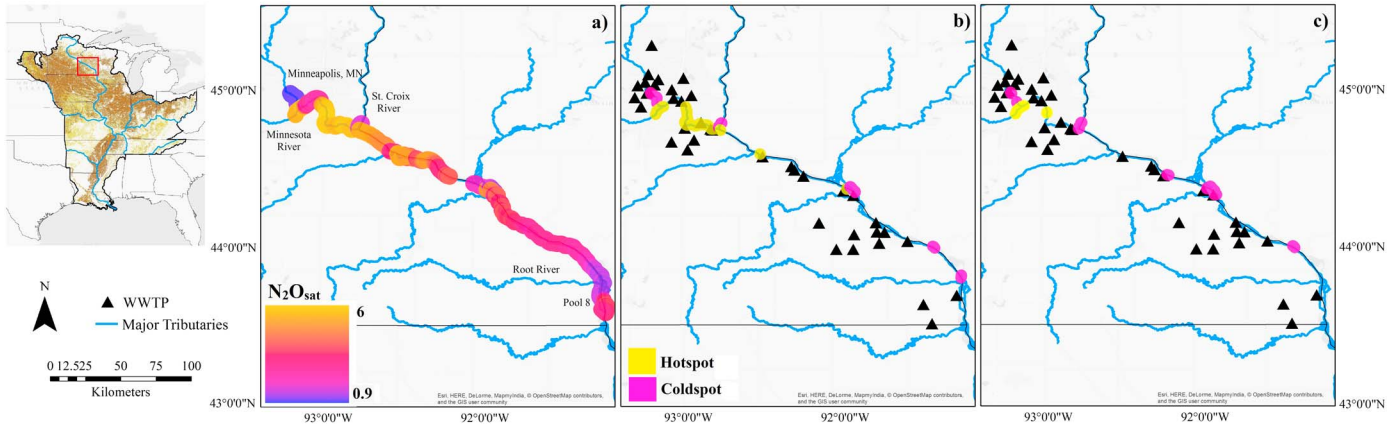

Figure 2. Inset: Agricultural land use within the UMR basin. Row crop (brown) and pasture (yellow) were drawn using information from the National Land Cover Database [*Xian et al.*, 2011]. (a) The regional-scale variability of N_2O_{sat} in the UMR ($n = 1553$). Hot spots and cold spots of (b) N_2O_{sat} and (c) NO_3^- concentrations.

Table 1. The Mean (Standard Deviation) of N_2O_{sat}, N_2O_{FLUX} (nmol N_2O N m^{-2} s^{-1}), NO_3^- (mg NO_3^- L^{-1}), DO (% Saturation), Chl *a* (Relative Fluorescence Units; RFU), Turbidity (Formain Nephelometric Units; FNU), fDOM (Quinine Sulfate Units; QSU), and Temperature (°C) During Each Sample Campaign

	Water Chemistry								
	N_2O_{sat}	N_2O_{FLUX}	NO_3^-	DO	Chl *a*	Turbidity	fDOM	pH	Temperature
Regional ($n = 1553$)	2.5 (0.9)	0.5 (0.2)	1.5 (1.3)	119.7 (16.4)	30.8 (12)	10.1 (6)	97 (13)	8.5 (0.2)	23.8 (0.6)
Pool 8—April ($n = 298$)	1.2 (0.1)	0.1 (0.06)	1.4 (1)	96.8 (3.2)	4.6 (2.1)	27.1 (35.8)	45.1 (11.3)	8.4 (0.2)	6.2 (0.7)
Pool 8—June ($n = 474$)	>4.8	>0.7	2 (1.5)	79 (9)	6.7 (2.5)	76.7 (81)	78 (27)	8 (0.5)	21 (0.4)
Pool 8—August ($n = 828$)	1.7 (0.3)	0.2 (0.1)	0.95 (1)	141.7 (32.6)	41.6 (20.3)	9.2 (4.8)	70.4 (21.7)	8.8 (0.3)	23.5 (0.9)
Pool 8—October ($n = 514$)	1.4 (0.2)	0.1 (0.06)	1.2 (0.6)	92.3 (5.6)	3.4 (1.3)	5 (1.6)	74.2 (17.3)	8.2 (0.1)	12 (0.7)

Spatial analyses, based on the Getis-Ord G* statistic [*Ord and Getis*, 2010], identified four N_2O_{sat} hot spots along this section of the UMR (Figure 2b). Hot spots were generally within close proximity to municipal wastewater treatment plants (WWTP). These hot spots dissipated rapidly, presumably because of dilution and outgassing over relatively short distances, suggesting that care should be taken when sampling nearby. The strength of these hot spots reflects differences in effluent discharge and river volume. Since NO_3^- hot spots were not observed downstream of each WWTP (Figure 2c), it is likely that N_2O was produced during wastewater processing prior to discharge into the UMR [*Kampschreur et al.,* 2009]. However, WWTPs are relatively minor contributors to the total N in the UMR, with greater than 70% being from agricultural sources [*Wall et al.,* 2013]. Our analyses identified five N_2O_{sat} cold spots (i.e., locations with anomalously low-dissolved N_2O) along this reach that were collocated with NO_3^- cold spots (Figure 2c), indicating that NO_3^- concentrations are an underlying requirement for N_2O production.

Overall, the surface water NO_3^- (RPI = 1) concentration was the most important explanatory variable driving regional fluctuations in UMR N_2O_{sat} (Figure 3a), whereas throughout the ice-free period, temperature (RPI = 1) and NO_3^- (RPI = 0.86) were the most important predictors (Figure 3b). The strong relation with NO_3^- throughout the UMR was expected because it is linked to both nitrification and denitrification. These processes are well documented in rivers [*Strauss et al.,* 2002; *Beaulieu et al.,* 2011], lakes [*Wang et al.,* 2009], reservoirs [*Beaulieu et al.,* 2015], and estuaries [*Owens*, 1986; *Murray et al.,* 2015]. In a well-oxygenated river such as the UMR, the strong relation between NO_3^- and N_2O_{sat} suggests that nitrification is a likely pathway to N_2O production [*Beaulieu et al.,* 2015]. This relationship also suggests that N_2O could be produced via denitrification, since the NO_3^- concentration in the surface water is likely an indirect measure of the NO_3^- available for diffusion into hypoxic sediments [*Rosamond et al.,* 2012], i.e., the sediment denitrification potential. Other processes (e.g., dissimilatory nitrate reduction to ammonia (DNRA) and nitrifier denitrification) may produce N_2O simultaneously, but the fluxes associated with these production pathways are expected to be small and cannot be elucidated from our data or analyses. However, the kinetics of NO_3^- processing and concurrent N_2O production are affected by secondary environmental factors—including turbidity (RPI = 0.4), pH (RPI = 0.3), fDOM (RPI = 0.18), and DO (RPI = 0.14)—that may limit or enhance reaction rates (production via nitrification and consumption via denitrification).

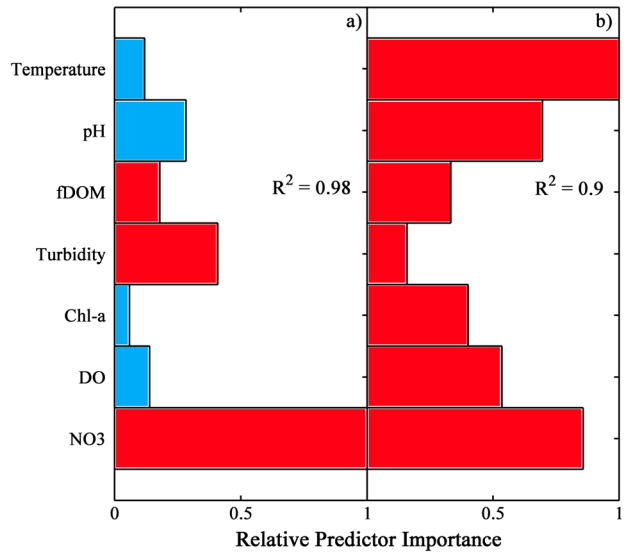

Figure 3. Relative predictor importance (RPI) determined using ensemble ($n = 500$) regression trees to predict N_2O_{sat} observations. Red and blue bars denote positive and negative relationships, respectively. The variable importance describes the explanatory power of a predictor on the N_2O_{sat} response. The pseudo R^2 was determined from an observed N_2O_{sat} versus predicted N_2O_{sat} relation from the ensemble regression model. Each value was normalized to the most important predictor in each system, (a) the RPI of the regional-scale measurements and (b) the temporal (April, August, and October) RPI from Pool 8.

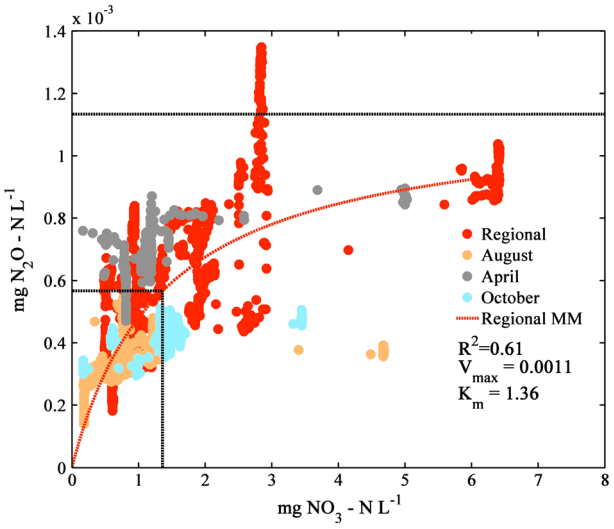

Figure 4. Measurements of N_2O and NO_3 from the UMR basin. The red dashed line is the Michaelis-Menten (MM) function derived from the regional-scale campaign ($n = 1553$). The black horizontal dashed line denotes the V_{max}, and the black dashed box represents the K_m.

We posit that these secondary factors indirectly dampen the N_2O_{sat} response by reducing the efficiency of NO_3^- removal (i.e., N_2O production potential) at high solute concentrations [*Mulholland et al.,* 2008]. This response has been attributed to limits on denitrification—including dissolved oxygen and carbon [*Mulholland et al.,* 2008]—that were also identified by our ensemble regression tree model. These data also classified pH as an important predictor, likely because it affects the rates of denitrification [*Knowles*, 1982] and nitrification [*Strauss et al.,* 2004]. We hypothesize that the positive relation identified between turbidity and N_2O_{sat} in the model reflects the fact that nitrifying bacteria bind to suspended particles in the water column [*Beaulieu et al.,* 2010]. Together, these factors affect the fraction of NO_3^- converted to N_2O at N saturation [*Beaulieu et al.,* 2011] that underlies the horizontal asymptote observed for dissolved N_2O concentrations in the UMR (Figure 4).

Using Michaelis-Menten kinetics [*García-Ruiz et al.,* 1998; *Boyer et al.,* 2006], we describe the weakening N_2O response to N saturation as

$$[N_2O] = \frac{V_{max} \times [NO_3^-]}{K_m + [NO_3^-]} \quad (5)$$

with the parameters estimated using a nonlinear least squares fitting function (*enzkin*; v. R2013B; Mathworks, Natick, MA, USA). Here the $[N_2O]$ (mg $N_2O-N\,L^{-1}$) can be derived from the $[NO_3^-]$ (mg $NO_3^-\,L^{-1}$) with a V_{max} of 0.0011 (95% CI; $\pm 4.1 \times 10^{-5}$) mg $N_2O-N\,L^{-1}$ and a K_m of 1.36 (±0.11) mg $NO_3^-\,L^{-1}$. The V_{max} represents the system's maximum $[N_2O]$ and the K_m is the $[NO_3^-]$ required to reach 50% of the V_{max}. The nonlinearity of Figure 4 implies that increasing NO_3^- concentrations will have a progressively weaker effect on N_2O concentrations in the UMR. In North America, river models project a doubling of the NO_3^- exported to estuaries by the year 2050 [*Seitzinger et al.,* 2002]. Using the relation shown in Figure 4, a doubling of NO_3^- would increase N_2O emissions from the UMR by about 42% (95% CI; 32–52%). Conversely, the U.S. Environmental Protection Agency has established a goal to reduce N export by 45% by 2035. If these goals were achieved, N_2O concentrations in the UMR would be decreased by about 32% (26–38%), implying a substantial reduction in N_2O emissions. However, because our regression tree models indicated that N_2O_{sat} was influenced by secondary factors, these forecasts could be diminished, for instance, a reduction in turbidity (decreased substrate for nitrifying bacteria) would lower N_2O_{sat} and therefore these forecasts should represent an upper estimate.

While automated soil N_2O measurement systems have become more common in recent years, techniques for continuous measurement of riverine N_2O concentrations have lagged behind. The techniques applied in this study have potential to address this problem worldwide and could significantly reduce the uncertainty in riverine N_2O emissions and the riverine emission factor (EF_{5r}) provided by the Intergovernmental Panel on Climate Change (IPCC) [*Nevison*, 2000]. For instance, stationary in situ sampling platforms located at strategic locations within a stream network could be used for emission upscaling [*Turner et al.,* 2015] to develop regionally appropriate, Tier II EF_{5r} values. Further, such data could be used to improve our understanding of the interannual variability and long-term dynamics of dissolved riverine N_2O and emissions.

4. Conclusions

Our data and analyses demonstrate that the UMR is supersaturated with N_2O during the ice-free period and is an important source of atmospheric N_2O. The regression tree models evaluated in this study indicate that NO_3^- is the dominant control on N_2O concentrations but that other environmental variables may limit NO_3^- processing. Given the significant nonlinear relation between NO_3^- and N_2O in the UMR, we expect that a doubling of N loading is likely to cause a substantial (32–52%) rise in dissolved N_2O concentrations and atmospheric emissions.

Acknowledgments
We thank William Breiter, Michael Dolan, Mark Dornblaser, Stephen Powers, and Matt Erickson for field and laboratory assistance. This work was supported by the U.S. Department of Agriculture, grant USDA-NIFA 2013-67019-21364, USDA-ARS, and the U.S. Geological Survey's LandCarbon program. Data are hosted at http://www.biometeorology.umn.edu/research/data-archives. Any use of trade or product names is for descriptive purposes only and does not imply endorsement by the U.S. Government.

References

Arévalo-Martínez, D. L., M. Beyer, M. Krumbholz, I. Piller, A. Kock, T. Steinhoff, A. Körtzinger, and H. W. Bange (2013), A new method for continuous measurements of oceanic and atmospheric N2O, CO and CO2: Performance of off-axis integrated cavity output spectroscopy (OA-ICOS) coupled to non-dispersive infrared detection (NDIR), *Ocean Sci.*, *9*(6), 1071–1087, doi:10.5194/os-9-1071-2013.

Arévalo-Martínez, D. L., A. Kock, C. R. Löscher, R. A. Schmitz, and H. W. Bange (2015), Massive nitrous oxide emissions from the tropical South Pacific Ocean, *Nat. Geosci.*, *8*, 530–533, doi:10.1038/ngeo2469.

Bange, H. W., S. Rapsomanikis, and M. O. Andreae (1996), Nitrous oxide emissions from the Arabian Sea, *Geophys. Res. Lett.*, *23*, 3175, doi:10.1029/96GL03072.

Baulch, H. M., S. L. Schiff, R. Maranger, and P. J. Dillon (2011), Nitrogen enrichment and the emission of nitrous oxide from streams, *Global Biogeochem. Cycles*, *25*, GB4013, doi:10.1029/2011GB004047.

Beaulieu, J. J., W. D. Shuster, and J. A. Rebholz (2010), Nitrous oxide emissions from a large, impounded river: The Ohio river, *Environ. Sci. Technol.*, *44*(19), 7527–7533, doi:10.1021/es1016735.

Beaulieu, J. J., C. T. Nietch, and J. L. Young (2015), Controls on nitrous oxide production and consumption in reservoirs of the Ohio River Basin, *J. Geophys. Res. Biogeosci.*, *120*, 1995–2010, doi:10.1002/2015JG002941.

Beaulieu, J. J., et al. (2011), Nitrous oxide emission from denitrification in stream and river networks, *Proc. Natl. Acad. Sci. U.S.A.*, *108*(1), 214–219, doi:10.1073/pnas.1011464108.

Boyer, E. W., R. B. Alexander, W. J. Parton, C. Li, K. Butterbach-Bahl, S. D. Donner, R. W. Skaggs, and S. J. Del Grosso (2006), Modeling denitrification in terrestrial and aquatic ecosytems at regional scales, *Ecol. Appl.*, *16*(6), 2123–2142, doi:10.1890/1051-0761(2006)016[2123:MDITAA]2.0.CO;2.

Cole, J. J., and N. F. Caraco (2001), Emissions of nitrous oxide (N2O) from a tidal, freshwater river, the Hudson River, New York, *Environ. Sci. Technol.*, *35*, 991–996.

Crawford, J. T., L. C. Loken, N. J. Casson, C. Smith, A. G. Stone, and L. A. Winslow (2015), High-speed limnology: Using advanced sensors to investigate spatial variability in biogeochemistry and hydrology, *Environ. Sci. Technol.*, *49*, 442–450.

Crawford, J. T., L. C. Loken, E. H. Stanley, E. G. Stets, M. M. Dornblaser, and R. G. Striegl (2016), Basin scale controls on CO2 and CH4 emissions from the Upper Mississippi River, *Geophys. Res. Lett.*, *43*, 1–7, doi:10.1002/2015GL067599.

De'ath, G., and K. E. Fabricius (2000), Classification and regression trees: A powerful yet simple technique for ecological data analysis, *Ecology*, *81*(11), 3178–3192, doi:10.1890/0012-9658(2000)081[3178:CARTAP]2.0.CO;2.

Food and Agriculture Organization (2015), FAOSTAT Database, *Food Agric. Organ. US*. [Available from: http://faostat3.fao.org/, Accessed 1 January 2016.]

Fassbinder, J. J., N. M. Schultz, J. M. Baker, and T. J. Griffis (2013), Automated, low-power chamber system for measuring nitrous oxide emissions, *J. Environ. Qual.*, *42*, 606–614, doi:10.2134/jeq2012.0283.

García-Ruiz, R., S. N. Pattinson, and B. A. Whitton (1998), Kinetic parameters of denitrification in a river continuum, *Appl. Environ. Microbiol.*, *64*(7), 2533–2538.

Grefe, I., and J. Kaiser (2014), Equilibrator-based measurements of dissolved nitrous oxide in the surface ocean using an integrated cavity output laser absorption spectrometer, *Ocean Sci.*, *10*, 501–512, doi:10.5194/os-10-501-2014.

Griffis, T. J., X. Lee, J. M. Baker, M. P. Russelle, X. Zhang, R. Venterea, and D. B. Millet (2013), Reconciling the differences between top-down and bottom-up estimates of nitrous oxide emissions for the U.S. Corn Belt, *Global Biogeochem. Cycles*, *27*, 746–754, doi:10.1002/gbc.20066.

Hartmann, D. L., et al. (2013), *Observations: Atmosphere and Surface*, edited by Intergovernmental Panel on Climate Change, Cambridge Univ. Press, New York.

Hinshaw, S. E., and R. A. Dahlgren (2013), Dissolved nitrous oxide concentrations and fluxes from the eutrophic San Joaquin River, California, *Environ. Sci. Technol.*, *47*, 1313–1322, doi:10.1021/es301373h.

Kampschreur, M. J., H. Temmink, R. Kleerebezem, M. S. M. Jetten, and M. C. M. van Loosdrecht (2009), Nitrous oxide emission during wastewater treatment, *Water Res.*, *43*(17), 4093–4103, doi:10.1016/j.watres.2009.03.001.

Knowles, R. (1982), Denitrification, *Microbiol. Rev.*, *46*(1), 43–70.

Lundy, M. E., C. M. Pittelkow, B. A. Linquist, X. Liang, K. J. van Groenigen, J. Lee, J. Six, R. T. Venterea, and C. van Kessel (2015), Nitrogen fertilization reduces yield declines following no-till adoption, *F. Crop. Res.*, *183*, 204–210, doi:10.1016/j.fcr.2015.07.023.

Marzadri, A., D. Tonina, A. Bellin, and J. L. Tank (2014), A hydrologic model demonstrates nitrous oxide emissions depend on streambed morphology, *Geophys. Res. Lett.*, *41*, 5484–5491, doi:10.1002/2014GL060732.

McMahon, P. B., and K. F. Dennehy (1999), N2O emission from a nitrogen-enriched river, *Environ. Sci. Technol.*, *33*(303), 21–25.

Miller, S. M., et al. (2012), Regional sources of nitrous oxide over the United States: Seasonal variation and spatial distribution, *J. Geophys. Res.*, *117*, D06310, doi:10.1029/2011JD016951.

Mulholland, P. J., et al. (2008), Stream denitrification across biomes and its response to anthropogenic nitrate loading, *Nature*, *452*(7184), 202–205, doi:10.1038/nature06686.

Murray, R. H., D. V. Erler, and B. D. Eyre (2015), Nitrous oxide fluxes in estuarine environments: Response to global change, *Glob. Chang. Biol.*, *21*, 3219–3245, doi:10.1111/gcb.12923.

Nevison, C. (2000), Review of the IPCC methodology for estimating nitrous oxide emissions associated with agricultural leaching and runoff, *Chemosph. Glob. Chang. Sci.*, *2*(3–4), 493–500, doi:10.1016/S1465-9972(00)00013-1.

Natural Resources Conservation Service (2012), Assessment of the effects of conservation practices on cultivated cropland in the Upper Mississippi River basin.

O'Reilly, C., I. R. Santons, T. Cyronak, A. McMahon, and D. T. Maher (2015), Nitrous oxide and methane dynamics in a coral reef lagoon driven by pore water exchange: Insights from automated high-frequency observations, *Geophys. Res. Lett.*, *42*, 2885–2892, doi:10.1002/2015GL063126.
Ord, J. K., and A. Getis (2010), Local spatial autocorrelation statistics: Distributional issues and an application, *Geogr. Anal.*, *27*(4), 286–306, doi:10.1111/j.1538-4632.1995.tb00912.x.
Owens, N. J. P. (1986), Estuarine nitrification: A naturally occurring fluidized bed reaction?, *Estuarine Coastal Shelf Sci.*, *22*, 31–44.
Panno, S. V., K. C. Hackley, W. R. Kelly, and H.-H. Hwang (2006), Isotopic evidence of nitrate sources and denitrification in the Mississippi River, Illinois, *J. Environ. Qual.*, *35*(2), 495–504, doi:10.2134/jeq2005.0012.
Rabalais, N. (2002), Nitrogen in aquatic ecosystems, *Ambio*, *31*(2), 102–112.
Ravishankara, A. R., J. S. Daniel, and R. W. Portmann (2009), Nitrous oxide (N2O): The dominant ozone-depleting substance emitted in the 21st century, *Science*, *326*, 123–125, doi:10.1126/science.1176985.
Richardson, W. B., E. A. Strauss, L. A. Bartsch, E. M. Monroe, J. C. Cavanaugh, L. Vingum, and D. M. Soballe (2004), Denitrification in the Upper Mississippi River: Rates, controls, and contribution to nitrate flux, *Can. J. Fish. Aquat. Sci.*, *61*(7), 1102–1112, doi:10.1139/f04-062.
Rosamond, M. S., S. J. Thuss, and S. L. Schiff (2012), Dependence of riverine nitrous oxide emissions on dissolved oxygen levels, *Nat. Geosci.*, *5*(10), 715–718, doi:10.1038/ngeo1556.
Santos, I. R., D. T. Maher, and B. D. Eyre (2012), Coupling automated radon and carbon dioxide measurements in coastal waters, *Environ. Sci. Technol.*, *46*, 7685–7691, doi:10.1021/es301961b.
Seitzinger, S. P., C. Kroeze, A. F. Bouwman, N. Caraco, F. Dentener, and R. V. Styles (2002), Global patterns of dissolved inorganic and particulate nitrogen inputs to coastal systems: Recent conditions and future projections, *Estuaries*, *25*(4), 640–655, doi:10.1007/BF02804897.
Spencer, R. G. M., G. R. Aiken, M. M. Dornblaser, K. D. Butler, R. M. Holmes, G. Fiske, P. J. Mann, and A. Stubbins (2013), Chromophoric dissolved organic matter export from U.S. rivers, *Geophys. Res. Lett.*, *40*, 1575–1579, doi:10.1002/grl.50357.
Strauss, E. A., N. L. Mitchell, and G. A. Lamberti (2002), Factors regulating nitrification in aquatic sediments: Effects of organic carbon, nitrogen availability, and pH, *Can. J. Fish. Aquat. Sci.*, *59*(3), 554–563, doi:10.1139/f02-032.
Strauss, E. A., W. B. Richardson, L. A. Bartsch, and J. C. Cavanaugh (2011), Effect of habitat type on in-stream nitrogen loss in the Mississippi River, *River Syst.*, *19*(3), 261–269, doi:10.1127/1868-5749/2011/019-0021.
Strauss, E. A., W. B. Richardson, L. A. Bartsch, J. C. Cavanaugh, D. A. Bruesewitz, H. Imker, J. A. Heinz, and D. M. Soballe (2004), Nitrification in the Upper Mississippi River: Patterns, controls, and contribution to the $NO3^-$ budget, *J. North Am. Benthol. Soc.*, *23*(3), 1–14.
Sutton, C. D. (2005), Classification and regression trees, bagging, and boosting, *Handb. Stat.*, *24*(04), 303–329, doi:10.1016/S0169-7161(04)24011-1.
Syakila, A., and C. Kroeze (2011), The global nitrous oxide budget revisited, *Greenh. Gas Meas. Manag.*, *1*(1), 17–26, doi:10.3763/ghgmm.2010.0007.
Turner, P. A., T. J. Griffis, X. Lee, J. M. Baker, R. T. Venterea, and J. D. Wood (2015), Indirect nitrous oxide emissions from streams within the US Corn Belt scale with stream order, *Proc. Natl. Acad. Sci. U.S.A.*, *112*(32), 9839–9843, doi:10.1073/pnas.1503598112.
Turner, R. E., and N. N. Rabalais (1991), Changes in Mississippi River water quality this century: Implications for coastal food webs, *Am. Inst. Biol. Sci.*, *41*(3), 140–147.
Venkiteswaran, J. J., M. S. Rosamond, and S. L. Schiff (2014), Nonlinear response of riverine N_2O fluxes to oxygen and temperature, *Environ. Sci. Technol.*, *48*(2), 1566–1573, doi:10.1021/es500069j.
Wall, D., D. Mulla, S. Weiss, D. Wasley, T. E. Pearson, and B. Henningsgaard (2013), *Nitrogen in Minnesota Surface Waters*, Minnesota Pollut. Control Agency, St. Paul, Minn.
Wallin, M. B., M. G. Öquist, I. Buffam, M. F. Billett, J. Nisell, and K. H. Bishop (2011), Spatiotemporal variability of the gas transfer coefficient (kCO2) in boreal streams: Implications for large scale estimates of CO2 evasion, *Global Biogeochem. Cycles*, *25*, GB3025, doi:10.1029/2010GB003975.
Wang, S., C. Liu, K. M. Yeager, G. Wan, J. Li, F. Tao, Y. Lü, F. Liu, and C. Fan (2009), The spatial distribution and emission of nitrous oxide (N2O) in a large eutrophic lake in eastern China: Anthropogenic effects, *Sci. Total Environ.*, *407*(10), 3330–3337, doi:10.1016/j.scitotenv.2008.10.037.
Wanninkhof, R. (1992), Relationship between wind speed and gas exchange over the ocean, *J. Geophys. Res.*, *97*, 7373–7382, doi:10.1029/92JC00188.
Weiss, R. F., and B. A. Price (1980), Nitrous oxide solubility in water and seawater, *Mar. Chem.*, *8*, 347–359, doi:10.1016/0304-4203(80)90024-9.
Xian, G., C. Homer, J. Dewitz, J. Fry, N. Hossain, and J. D. Wickham (2011), Completion of the 2011 National Land Cover Database for the conterminous United States—Representing a decade of land cover change information, *Photogramm. Eng. Remote Sensing*, *77*(8), 758–762.
Yoon, T. K., H. Jin, N.-H. Oh, and J.-H. Park (2016), Technical note: Applying equilibration systems to continuous measurements of pCO2 in inland waters, *Biogeosci. Discuss.*, doi:10.5194/bg-2016-54.